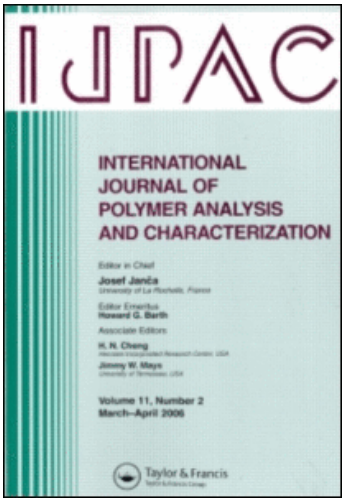

International Journal of Polymer Analysis and Characterization
Publication details, including instructions for authors and subscription information:
http://www.informaworld.com/smpp/title~content=t713646643

Synthesis and Characterization of Colloidal Crystal Array of Polystyrene-Hydrophilic Monomer Microgels

Pandya Prashant[a]; Seong S. Seo[a]
[a] Department of Natural Sciences, Albany State University, Albany, Georgia, USA

Online publication date: 01 February 2010

To cite this Article Prashant, Pandya and Seo, Seong S.(2010) 'Synthesis and Characterization of Colloidal Crystal Array of Polystyrene-Hydrophilic Monomer Microgels', International Journal of Polymer Analysis and Characterization, 15: 2, 98 — 109
To link to this Article: DOI: 10.1080/10236660903474464
URL: http://dx.doi.org/10.1080/10236660903474464

International Journal of Polymer Anal. Charact., 15: 98–109, 2010

ISSN: 1023-666X print
DOI: 10.1080/10236660903474464

Taylor & Francis
Taylor & Francis Group

SYNTHESIS AND CHARACTERIZATION OF COLLOIDAL CRYSTAL ARRAY OF POLYSTYRENE-HYDROPHILIC MONOMER MICROGELS

Pandya Prashant and Seong S. Seo
Department of Natural Sciences, Albany State University, Albany, Georgia, USA

We developed a new photonic colloidal crystal array based on hydrophobic monomer styrene (St) and hydrophilic monomers acrylic acid (AAc), methacrylic acid (MAc), and itaconic acid (IAc) by free radical emulsion polymerization method. These StlAAc, StlMac, and StlIAc nanoparticles were characterized with respect to particle size by SEM. Reflectance microscopy was utilized to monitor structural changes during the self-assembly of monodispersed colloidal systems at room temperature. Three different monomers gave three different particle sizes, 159.9 nm, 280.7 nm, and 255.8 nm for StlAAc, StlMac, and StlIAc microgel, respectively. Difference in particle size arises due to the change in monomer molecular weight, 72.06, 86.09, and 130.1 for AAc, Mac, and IAc respectively. These monodispersed, spherical colloidal particles that rapidly self-assemble via simple solvent evaporation to form 3-D colloidal crystals are both robust and uniformly diffractive. SEM analysis revealed the hexagonal particle shape of StlAAc and square shape of StlIAc. As crystals dry, they assist in particle self-assembly to form an ordered structure. These dried, colloidal crystal arrays exhibit Bragg diffraction, which can be modified by changing monomer types acrylic acid, methacrylic acid, and itaconic acid. This unique approach can be used as processable emulsions, which can be used for the preparation of materials for chemical sensors. These microgels if functionalized with calcium could be used as a potential sensor for organophosphate nerve agent like paraoxon.

***Keywords*:** Colloidal crystal array; Microgels; Reflectance measurement

INTRODUCTION

Latex polymer colloids are important in many areas of technology, such as paint and coatings, ceramics processing, and biotechnology.[1] These particles are often prepared by emulsion polymerization, which can produce highly monodisperse spherical particles from polymers such as polystyrene and polymethylmethacrylate. A group from Dow Chemical Corp. was the first in 1947 to demonstrate the synthesis of monodisperse polystyrene latex colloids.[2] The remarkable size

Submitted 8 October 2009; accepted 9 November 2009.
This work was supported by grants from the National Institutes of Health, RIMI program, Grant P20 MD001085, and the Department of Defense, Grant W911NF-06-1-0433, whose support is greatly appreciated.
Correspondence: Seong S. Seo, Department of Natural Sciences, Albany State University, 504 College Dr., Albany, GA 31705, USA. E-mail: ssseo@asurams.edu

uniformity of these colloids was demonstrated in the early electron microscopy studies.[3] This work was followed by demonstration of different synthetic approaches that produce monodisperse colloidal particles. These approaches include emulsion polymerization, seeded emulsion polymerization, emulsifier free polymerization, precipitation polymerization, and dispersion polymerization.[4–8] At high particle concentrations, these monodisperse particles form highly ordered closely packed structures that diffract light. The closely packed structures often show a random stacked hexagonal ordering. Alfrey et al.[9] were the first to study the light-scattering properties of colloidal crystal arrays (CCAs) and showed that these crystals efficiently diffract light. This CCA Bragg diffraction result is a unique optical phenomenon that gives these materials interesting applications in optics and spectroscopic instruments.

Colloidal self-assembly (CSA) is a bottom-up method for fabricating highly ordered 2-D and 3-D nanostructures. This method has the advantage over the conventional top-down method of fabrication because the process is highly parallel. Colloids are also an excellent model system for the study of atomic systems because the length and time scales of the colloids system are easily accessible experimentally. The nanostructures obtained by self-assembly known as colloidal crystals have enormous potential for photonics[10–12] and biological[13] applications. Monodispersed spherical particles have been investigated extensively for their use in the fabrication of colloidal crystals and for the design of optical materials.[14] For example, ordered structures have been shown to exhibit photonic band gap behavior.[15,16] The investigation of these materials has established their use in many optical applications such as wave guides,[17,18] filters, switches, and sensing devices.[19,20] To produce colloidal crystals that can achieve these functions, it is necessary to maintain control over the assembly of the particles to afford reproducibility and to minimize structural defects that can diminish the optical properties of the material. Self-assembly approaches offer a distinct advantage in that they are efficient, require minimal fabrication efforts, and can be easily modified for widespread manufacturing purposes. However, such approaches are intrinsically tied to obtaining thermodynamic control over assembly, which often requires very slow assembly or sedimentation to limit the number and size of kinetically trapped defects. A self-assembly technique that is appropriate for creating processable materials should be quick and simple and provide a crystalline construction that possesses a high degree of stability, so that it would be useful for many optical applications.[21,22]

Many types of self-assembly-based fabrication strategies have been explored to produce colloidal crystals. Some of the simplest techniques include sedimentation and centrifugation procedures. Many diverse methods have been investigated to enhance speed of crystal formation through controlled processes. Capillary deposition,[23] vertical deposition,[24,25] convective assembly,[26] spin coating,[27] electrophoretic assembly,[28,29] and other innovative designs[30,31] have been investigated for the purposes of controlling the extent and orientation of crystalline order as well as crystal thickness. However, these methods often require complex configurations or long deposition times that are essential for crystal formation. Simple methods that make use of solvent evaporation have been also explored, and the dynamics of these assembly interactions has been widely investigated.[32–34] Despite the potential of CSA, in situ monitoring of structural changes during the

CSA process is still not well understood. The reason is that the process occurs by a change of the environment from solvent to air. Although the equilibrium behavior of colloids in solvent has been extensively studied, the change of the environment involves a nonequilibrium process. During CSA, the liquid-vapor interface closes in and confines the colloids into closed-pack structures. This causes large distortive capillary forces that propagate through the colloidal crystal and affects the CSA process profoundly. Lateral capillary forces acting on colloid particles in 2-D array have been experimentally and theoretically studied.[35] However, the studies have not been extended to 3-D arrays and their collective behavior.

For monodisperse colloids in solvent, it has been found that the close-pack face-centered cubic (FCC) structure is the equilibrium structure.[36] This behavior is good for CSA because the capillary forces tend to pack the colloids closely, and the FCC colloidal crystals will undergo less distortion in their lattice during the drying process. However, non-closely pack structures can also occur in equilibrium under different conditions. For example, ionic colloidal crystal has been reported.[37] In this case, the capillary forces may distort the structure severely and break up the structure. Thus, the actions of capillary forces on such 3-D arrays of particles need to be understood. It will then be helpful to observe the structural changes during CSA.

In this work, we have synthesized spherical nanoparticles composed of poly(styrene-co-acrylic) acid (St/AAc), poly(styrene-co-methacrylic) acid (St/MAc), and poly(styrene-co-itaconic) acid (St/IAc) by the surfactant-free emulsion polymerization method, which can be used to obtain robust, 3-D colloidal crystalline materials via the facile method of solvent evaporation under ambient conditions. All reactions were carried out at 70°C under inert atmosphere for 6 h. The particles were characterized with respect to particle size distribution by scanning electron microscopy (SEM) analysis. We prepared CCA after centrifugation of three different emulsions as stated above at 20000 RPM for 2 h, two times. Three different monomers, AAc, Mac, and IAc, gave three different particle sizes, 159.9 nm, 280.7 nm, and 255.8 nm, due to the change in molecular weight of polymerizing monomers 72.06, 86.09, and 130.1 g/mol, respectively. CCAs were prepared by the double-gasket method, and in situ monitoring of reflectance was carried out at room temperature over a period of 45 min for St/IAc, St/Mac, and St/IAc nanoparticles. The nanoparticles provided the basic material for quick crystal formation that can be adapted toward processable crystal. We observed a change of reflectance peak from 569 to 545 nm, from 694 to 639 nm, and from 758 to 736 nm for St/AAc, St/Mac, and St/IAc microgels, respectively. SEM analysis revealed the ordered structure of the nanoparticles, confirming CCA formation. Addition of acrylic acid, methacrylic acid, and itaconic acid mainly adds soft qualities that provide particle flexibility to some extent but not thermosensitivity. The crystalline order is maintained by mainly hard polystyrene, ultimately affording a stable, ordered configuration.

EXPERIMENTAL SECTION

Materials and Methods

Styrene, acrylic acid, methacrylic acid, itaconic acid, ammonium persulfate (APS), and N-N-methylenebis (acrylamide) (BIS) were purchased from Sigma

Aldrich and used as received. Distilled water was purified to a resistance of 18 MΩ and then filtered through a 0.2 μm filter to remove particulate matter.

Nanoparticle Syntheses

Poly(styrene-co-acrylic acid) (St/AAc), poly(styrene-co-methacrylic) acid (St/MAc), and poly(styrene-co-itaconic) acid (St/IAc) synthesis was performed using a one-pot, surfactant-free emulsion polymerization method.[38] In the process, 0.020 mol of styrene, 0.007 mole of IAc, and 0.0003 mole of BIS were used. For the synthesis, AAc and BIS were dissolved in 100 mL of water, and the reaction mixture was heated to 70°C and purged with nitrogen for 75 min in a three-necked round-bottomed flask equipped with a condenser and inlet for nitrogen with constant stirring. The styrene was added just prior to initiation. Initiation was performed by using 0.027 mol of APS, which was pre-dissolved in 0.5 mL of water. An additional amount of APS (0.044 mmol) was added to ensure reaction completion. After 4 h of constant stirring, with the temperature maintained at 70°C, the reaction solutions were filtered using Whatman filter paper (no. 2) to remove any solutions and cleaned by centrifuging two times for approximately 2 h at 20000 RPM at 25°C to remove any unreacted monomer or oligomeric species, using distilled deionized water. St/MAc and St/IAc nanoparticles were prepared by the same method as described above.

Particle Size Analysis

Particle size of St/AAc, St/Mac, and St/IAc were determined by a Beckmann Coulter particle size analyzer at 25°C at an angle of 90°. Each measurement consisted of five data points. The average particle sizes for all three nanoparticles were 159.9 nm, 280.7 nm, and 255.8 nm for St/AAc, St/Mac, and St/IAc, respectively.

Colloidal Crystal Array Preparation

To prepare CCA, 1.5 μL of St/AAc was centrifuged and the nanoparticles were dropped over a 0.2 mm thick double-sided gasket. Reflectance spectra were recorded over a period of 50 min. In this manner, reflectance spectra of St/MAc and St/IAc nanoparticles were also recorded.

Reflectance Spectroscopic Analysis

Reflectance spectroscopy of dried crystals was performed using an Ocean Optics USB 4000 spectrophotometer operating in the range of 100–1000 nm using an integrating sphere accessory and the accompanying scan package.

Scanning Electron Microscopy Analysis

Scanning electron microscopy (SEM) was used to characterize the structural properties of dried samples of St/AAc and St/IAc particles. The samples for SEM analysis were prepared by drying a concentrated suspension of particles on a glass

coverslip, onto which a 5 nm gold film was added using a vacuum evaporator. Samples were placed on a flat, cylindrical specimen mount for imaging the top of the dried sample. To obtain images of a sample cross section, a drop of particle suspension was dried on a scored glass coverslip. After the sample dried completely, the coverslip was broken along a scored line, followed by deposition of a gold film, as described above. A 45° specimen mount was used for obtaining images of the crystal cross section by tilting the sample relative to the incident electron beam. The LEO 982 field emission scanning electron microscope (FE-SEM, LEO Electron Microscopy, Inc., Thornwood, New York) provides a means to achieve ultrahigh resolution images in the secondary emissive mode. The instrument is, in fact, an analytical workstation since it combines secondary imaging capabilities with backscatter electron imaging useful for discriminating elements by atomic number contrast.

RESULTS AND DISCUSSION

Three different sizes of nanoparticles were prepared using three different monomers, acrylic acid, methacrylic acid, and itaconic acid copolymerizing with styrene. They were used separately for the fabrication of dried colloidal crystals. The nanoparticles were prepared using a feed of 73% styrene, 26% acrylic acid, and 1% BIS. In this manner, polystyrene-co-methacrylic acid and polystyrene-co-itaconic acid nanoparticles were also prepared. A particle size analyzer was used to determine the particle size by suggesting that as the hydrophilicity of monomer increases,[39] particle size also increases, which can be clearly observed from Table I. To characterize the final colloidal crystal product that is formed from nanoparticles of St/AAc, St/Mac, and St/IAc, the properties of the constituent particles were examined by a dynamic light scattering analyzer (DLS). Variation of the monomers used in the synthesis of three different particles was found to affect the particle size, as demonstrated using particle size analysis. The light scattering data demonstrate the narrow difference for these nanoparticles, which is essential for the assembly of crystalline lattices using spherical particles. As shown in Table I, significant increase in particle size was observed. It is reported[40] that it is difficult to estimate the arrangement of homopolymer-rich regions of particles based on the reactivity ratios of styrene and acrylic acid, methacrylic acid, and itaconic acid. When hydrophilic monomers polymerize with styrene, it has been shown that the exterior of the particles is composed mostly of the more hydrophilic monomer due to some degree of phase separation, while the interior of the particle consists of more hydrophobic polystyrene.[41,42] Therefore it is proposed that this change in particle size is due primarily to the loss of solvent from the hydrated acrylic, methacrylic, and itaconic-rich periphery of the particle, while the spherical shape is effectively preserved as a result of dense polystyrene-rich core. The variation in size indicates the extent of surface flexibility that can be realized with these copolymer particles.

Table I. Particle size characterization

St/AAc	St/MAc	St/IAc
159.9 ± 2.8	280.7 ± 2.6	255.8 ± 6.2

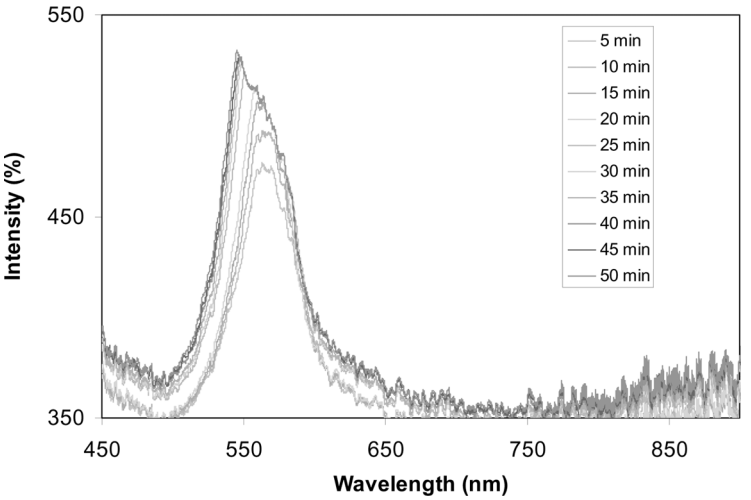

Figure 1. In situ measurement of reflectance: polystyrene-acrylic acid nanoparticles.

We prepared colloidal crystal arrays of three different nanoparticles by the double-gasket method. Reflectance spectroscopy was employed to determine the wavelength of Bragg diffraction for these crystalline materials. Colloidal crystalline arrays of St/AAc, St/Mac, and St/IAc exhibit first-order diffraction at 569, 694, and 758 nm respectively as shown in Figures 1, 2, and 3, respectively. Scanning electron microscopy was used to image the particle order of the dried nanoparticle samples. The three-dimensional order of the St/AAc, St/Mac, and St/IAc is

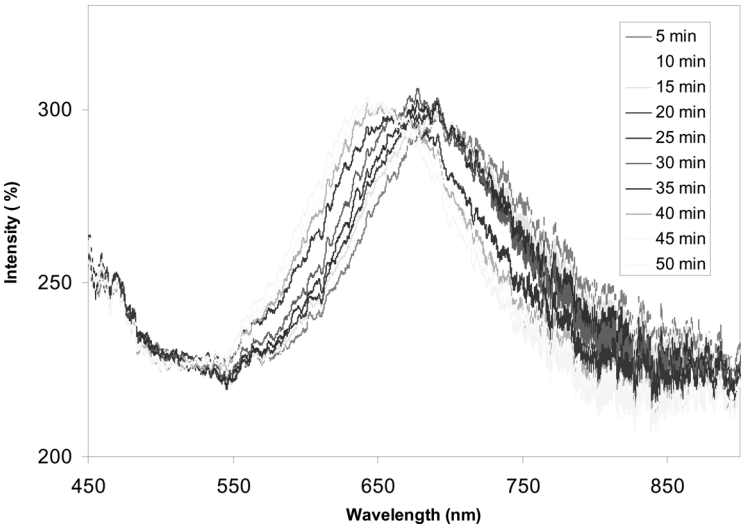

Figure 2. In situ measurement of reflectance: polystyrene-methacrylic acid nanoparticles.

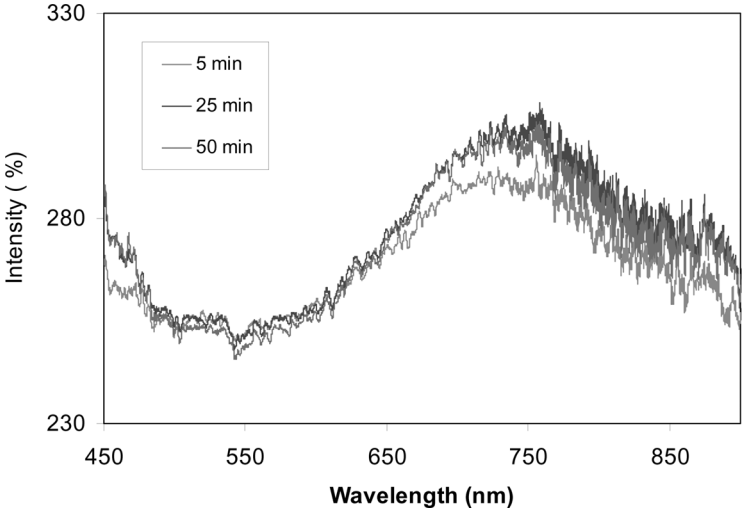

Figure 3. In situ measurement of reflectance: polystyrene-itaconic acid nanoparticles.

revealed by imaging the sample along cracks or a sample cross section. It is apparent from these images that the samples are well ordered.

The CCA formation process can be separated into three different stages[43]: the constant rate period, the first falling rate period, and the second falling rate period. First is the constant rate period, in which the decrease in volume of the particle network is equal to the volume of liquid lost by evaporation, that is, in which the rate of evaporation per unit area of the drying surface is independent of time. The stress drying film reaches its maximum value at the surface of the film at a critical point at the end of this constant rate period. At this point, shrinkage stops as a continuous rigid networks of particles is formed. This is when cracking is most likely to occur because of the stress difference between the wet and dry parts of the body as the drying front moves toward the interior of the body. The likelihood of cracking is greater for a thin film that dries on a flat right substrate. Also, at this point, air starts entering the pores. The saturated body is translucent or transparent because of the similarity in refractive index of the liquid and solid, but the lower index of air causes significant scattering of light. The drained regions may be big enough to scatter the light, even if the ores themselves are too small to do so, explaining why films turn opaque during the falling rate periods, while they are transparent when fully saturated or fully dried. Looking at Figure 4, we observe that constant rate period is up to 25 min for St/AAc and St/Mac and 50 min for St/IAc nanoparticles in peak wavelength shift with a function of time.

The falling rate period starts after 25 min for St/AAc and St/MAc and 50 min for St/IAc nanoparticles as shown in Figure 4. We can say that initially the solvent evaporates faster up to 25 min. After 25 min, the rate of evaporation becomes slower. This could be due to respective hydrophilicity of the nanoparticles. Upon drying this colloidal crystal array, it was observed that the edge of the substrate began to exhibit iridescent color after a few minutes and the iridescent color gradually moved from the periphery toward the center of the substrate. When we took square-shaped glass

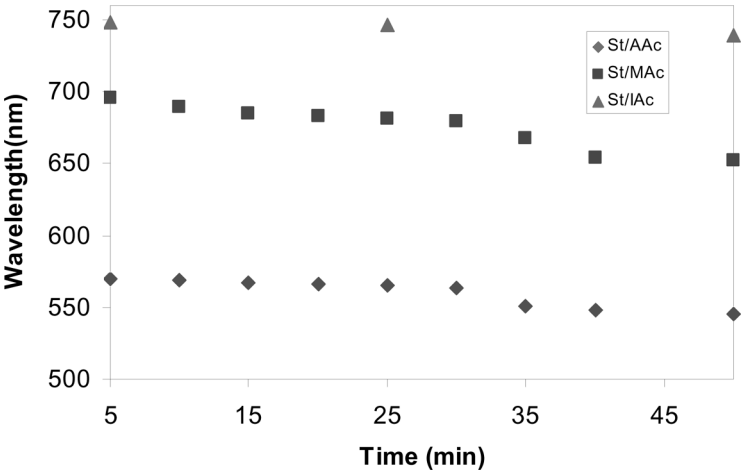

Figure 4. Comparative drying effects on peak wavelength shift.

slides, it took around 50 min to complete crystallization under ambient conditions. Interestingly, a macroscopic circular void can be seen. Further void was observed to be located in the center of the film or the substrate. The presence of void is a strong indication of the mechanism of colloidal crystal growth.

To characterize the CCA formation process, in situ reflectance spectroscopy was performed as a drop of nanoparticle was allowed to dry. The reflectance probe was positioned at a 90° angle above the drop and about half way between the center of the drop and its edge. Reflectance spectra, as shown in Figures 1–3, were collected as the drop dried over a period of 50 min. As the sample dried, an initial diffraction peak was observed at 569, 694, and 758 nm for St/AAc, St/Mac, and St/IAc nanoparticles, respectively, that is red-shifted. The intensity of the initial peaks increases and becomes shifted over time during evaporation. As shown in Figures 1–3, the colors of the spectra correspond to different times throughout the CCA formation process, which occurred on the order of minutes. The peaks were shifted from left to right, suggesting that solvent was evaporating out from nanoparticles, and as per the Bragg law the distance between the particles was decreasing and, simultaneously, the wavelength was also decreasing. Further looking at the reflectance in Figures 1–3, we can say that first there is an evolution of the peak due to the ordered structure, and the crystal size decreases, showing the peak moving from right to left as per Bragg diffraction. The gradual shift in peak wavelength indicates that the lattice of the FCC structure is shrinking over a period of time.

Further, from Figure 4, we can say that there is an important shift of peak wavelength for St/AAc, St/MAc, and St/IAc nanoparticles after 25, 25, and 50 min, respectively. For St/AAc we observed a peak shift from 570 to 560 nm within 25 min of drying, and after 25 min its fast shifting means that more and more solvent is going out of the nanoparticles. Looking at Figure 4 for St/Mac nanoparticles, peak shift was observed within 25 min from 695 to 680 nm, later on, as compared

to St/AAc, there was dramatic change in peak wavelength from 675 to 650 nm, which suggested the same phenomenon of more hydrophobicity due to which the solvent comes out of the nanoparticles very rapidly. Looking at Figure 4 for St/IAc nanoparticles, we observe peak shift from 748 to 738 nm, suggesting that these nanoparticles are more hydrophilic, due to which it takes more time for solvent to evaporate out of St/IAc nanoparticles than out of St/AAc and St/MAc nanoparticles.

Crystalline quality is among the most important parameters in determining the performance of colloidal crystals in optical applications. The formation of point

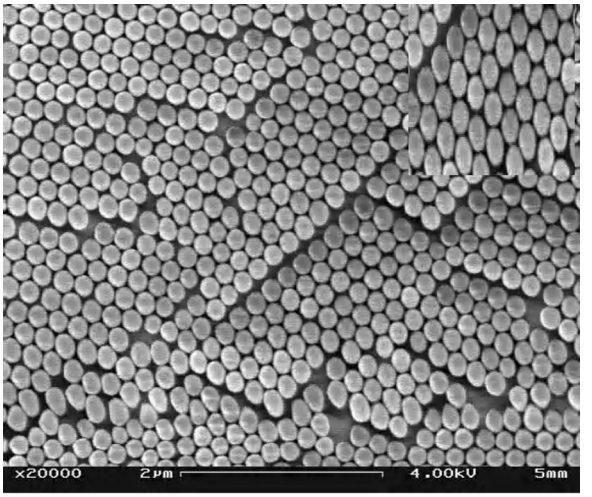

(a)

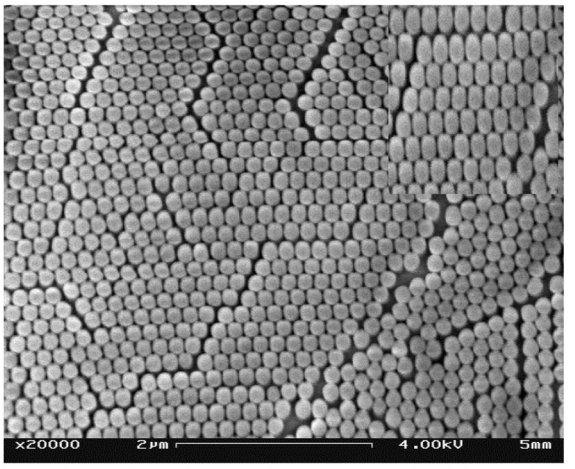

(b)

Figure 5. (a) SEM analysis of styrene/acrylic acid nanoparticles (inset: hexagonal particle); (b) styrene/itaconic acid nanoparticles (inset: square particle).

defects or domains can have an enormous impact on the diffraction properties. Figures 5(a) and (b) shows typical SEM images of a single crystal of colloidal St/AAc and St/IAc. These samples exhibit an ordered arrangement of colloids. One interesting feature we observe is that particles are of hexagonal shape like benzene ring for St/AAc colloids as shown in Figure 5(a), whereas looking at Figure 5(b), we observe regular arrangement of nanoparticles, and, interestingly, these St/IAc particles have a perfect square shape, as shown in Figure 5(b). It is a challenge to use microscopy for proof of sample order.

To form high quality crystals, particle size is a crucial factor. This is illustrated in Table I and Figures 5(a) and (b), as we observe that particle size of St/AAc, 152.9 nm, is smaller than particle size of St/IAc, 255.8 nm. The sample with narrow distribution exhibits order over a long length scale and sharp arrangement. Further, particle size affects the film thickness in a systematic way: for the same volume fraction, a solution of larger particles yields fewer layers. SEM images of the top view of these samples show that the colloids are arranged in a closely packed fashion, with each sphere touching six others in one layer (Figures 5(a) and (b)). This closely packed arrangement is well-known arrangement in crystal comprised in colloids. In this closely packed geometry, whether the structure is face-centered cubic, hexagonal closely packed, or randomly stacked, these images illustrate that the samples are oriented with their axes parallel to the substrate. Exact characterization of the crystal structure of these samples from SEM micrographs alone is problematic. Although images such as these confirm a regular closely packed arrangement, they cannot be used to distinguish between fact and hexagonal closely packed (hcp) structures. This is because it is difficult to determine the exact angle of the cross-sectional view, which in turn makes it difficult to assess which crystal face is visualized in these images.

CONCLUSION

We synthesized three different novel nanoparticles, St/AAc, St/Mac, and St/IAc, based on the emulsifier free emulsion polymerization method. Colloidal crystal arrays prepared from these particles exhibit Bragg diffraction; self-assembly occurred via simple solvent evaporation. Three different hydrophilic monomers resulted in three different particle sizes depending upon their hydrophilic nature and softness. The nanoparticles afforded a degree of softness that allowed for particle ordering, while also possessing hard sphere qualities based on polystyrene that provided final crystalline stability when fully dried. The nanoparticles were characterized with respect to particle size distribution by scanning electron microscopic analysis and reflectance spectroscopic analysis. SEM and reflectance spectroscopy demonstrated the extent of crystalline order. In situ reflectance spectroscopy was used to show that hydrated nanoparticles initially become ordered, and as they lose water via evaporation, their particle size decreases while the crystalline order is retained. Variations in the hydrophilicity of the monomers and particles prepared could be used to alter the structure of the colloidal particles, as well as the optical properties of the final crystal. This simple colloidal crystal array could be constructed as a potential organophosphate nerve agent sensor if functionalized with calcium.

REFERENCES

1. Fitch, R. M. (1997). *Polymer Colloids*. San Diego: Academic Press.
2. Krieger, I. M., and F. M. O'Neill. (1968). Diffraction of light by arrays of colloidal spheres. *J. Am. Chem. Soc.* **90**, 3114–3120.
3. Backus, R. C. (1948). Program of the E. F. Burton memorial meeting of the electron microscope society of America. *J. Appl. Phys*. **19**(12), 1186–1193.
4. Matijevic, E. (1986). Monodispersed colloids: Art and science. *Langmuir* **2**, 12.
5. Harkins, W. D. (1947). A general theory of the mechanism of emulsion polymerization. *J. Am. Chem. Soc.* **69**, 1428–1444.
6. Tsuar, S. L., and R. M. Fitch. (1987). Preparation and properties of polystyrene model colloids: I. Preparation of surface-active monomer and model colloids derived therefrom. *J. Colloids Interface Sci.* **115**, 450–462.
7. Chang, S., L. Liu, and S. A. Asher. (1994). Creation of templated complex topological morphologies in colloidal silica. *J. Am. Chem. Soc.* **116**, 6745–6747.
8. Rempp, P., and E. W. Merrill. (1986). *Polymer Synthesis*. Basel: Huthig and Wepf Verlag.
9. Alfrey, T., E. B. Bradford, and J. W. Vanderhoff. (1954). Optical properties of uniform particle-size latexes. *J. Opt. Soc. Am.* **44**, 603–607.
10. Lopez, C. (2003). Materials aspects of photonic crystals. *Adv. Mater.* **15**, 1679–1704.
11. Lu, Y., Y. Yin, and Y. Xia. (2001). Preparation and characterization of micrometer-sized egg shells. *Adv. Mater.* **13**, 271–274.
12. Stein, A., and R. C. Schroden. (2001). Colloidal crystal templating of three-dimensionally ordered macroporous solids: Materials for photonics and beyond. *Curr. Opin. Solid State Mater. Sci.* **5**, 553–564.
13. Kotov, N. A., Y. Liu, S. Wang, C. Cumming, M. Eghtedari, G. Vargas, M. Motamedi, J. Nichols, and J. Cortiella. (2004). Inverted colloidal crystals as three-dimensional cell scaffolds. *Langmuir* **20**, 7887–7892.
14. Xia, Y., B. Gates, Y. Yin, and Y. Lu. (2000). Monodispersed colloidal spheres: Old materials with new applications. *Adv. Mater.* **12**, 693–713.
15. Joannopoulos, J. D., and P. R. Villeneuve. (1997). Photonic crystals: Putting a new twist on light. *Nature* **387**, 830.
16. Yablonovitch, E. J. (1993). Photonic band-gap structures. *J. Opt. Soc. Am. B* **10**, 283–295.
17. Lee, W., S. A. Pruzinsky, and P. V. Braun. (2002). Multi-photon polymerization of waveguide structures within three-dimensional photonic crystals. *Adv. Mater.* **14**, 271–274.
18. Li, J., P. R. Herman, C. E. Valdivia, V. Kitaev, and G. A. Ozin. (2005). Colloidal photonic crystal cladded optical fibers: Towards a new type of photonic band gap fiber. *Opt. Express* **13**, 6454–6459.
19. Holtz, J. H., and S. A. Asher. (1997). Polymerized colloidal crystal hydrogel films as intelligent chemical sensing materials. *Nature* **389**, 829–832.
20. Alper, J. (2006). Massively parallel single-cell analyses. *Anal. Chem.* **78**, 5249–5250.
21. Noris, D. J., E. G. Arlinghaus, L. Meng, R. Heiny, and L. E. Scriven. (2004). Opaline photonic crystals: How does self-assembly work? *Adv. Mater.* **16**, 1393–1399.
22. Xia, Y., B. Gates, and Z.-Y. Li. (2001). Self-assembly approaches to three-dimensional photonic crystals. *Adv. Mater.* **13**, 409–413.
23. Li, H.-L., and F. Marlow. (2006). Solvent effects in colloidal crystal deposition. *Chem. Mater.* **18**, 1803–1810.
24. Jiang, P., J. F. Bertone, K. S. Hwang, and V. L. Colvin. (1999). Single-crystal colloidal multilayers of controlled thickness. *Chem. Mater.* **11**, 2132–2140.

25. Li, J., and Y. Han. (2006). Optical intensity gradient by colloidal photonic crystals with a graded thickness distribution. *Langmuir* **22**, 1885–1890.
26. Wostyn, K., Y. Zhao, B. Yee, K. Clays, A. Persoons, G. De Schaetzen, and L. Hellemans. (2003). Optical properties and orientation of arrays of polystyrene spheres deposited using convective self-assembly. *J. Chem. Phys.* **118**, 10752–10758.
27. Jiang, P., and M. J. McFarland. (2004). Large-scale fabrication of wafer-size colloidal crystals, macroporous polymers and nanocomposites by spin-coating. *J. Am. Chem. Soc.* **126**, 13778–13786.
28. Trau, M., D. A. Saville, and I. A. Aksay. (1996). Field-induced layering of colloidal crystals. *Science* **272**, 706–709.
29. Rogach, A. L., N. A. Kotov, D. S. Koktysh, J. W. Ostrander, and G. A. Ragoisha. (2000). Electrophoretic deposition of latex-based 3D colloidal photonic crystals: A technique for rapid production of high-quality opals. *Chem. Mater.* **12**, 2721–2726.
30. Park, S. H., and Y. Xia. (1999). Assembly of mesoscale particles over large areas and its application in fabricating tunable optical filters. *Langmuir* **15**, 266–273.
31. Wong, S., V. Kitaev, and G. Ozin. (2003). Colloidal crystal films: Advances in universality and perfection. *J. Am. Chem. Soc.* **125**, 15589–15598.
32. Okubo, T., K. Kimura, and H. Kimura. (2002). Dissipative structures formed in the course of drying the colloidal crystals of monodispersed polystyrene spheres on a cover glass. *Colloid Polym. Sci.* **280**, 1001–1008.
33. Koh, Y. K., and C. C. Wong. (2006). In situ monitoring of structural changes during colloidal self-assembly. *Langmuir* **22**, 897–900.
34. Juillerat, F., P. Bowen, and H. Hofmann. (2006). Formation and drying of colloidal crystals using nanosized silica particles. *Langmuir* **22**, 2249–2257.
35. Kralchevsky, P. A., and K. Nagayama. (2000). Capillary interactions between particles bound to interfaces, liquid films and biomembranes. *Adv. Colloid Interface Sci.* **85**, 145–192.
36. Sirota, E. B., H. D. Ou-Yang, S. K. Sinha, P. M. Chaikin, J. D. Axe, and Y. Fujii. (1989). Complete phase diagram of a charged colloidal system: A synchrotron x-ray scattering study. *Phys. Rev. Lett.* **62**, 1524–1527.
37. Leunissen, M. E., C. G. Christova, A.-P. Hynninen, C. P. Royall, A. I. Campbell, A. Imhof, M. Dijkstra, R. van Roij, and A. van Blaaderen. (2005). Ionic colloidal crystals of oppositely charged particles. *Nature* **437**, 235–240.
38. Hellweg, T., C. D. Dewhurst, W. Eimer, and K. Kratz. (2004). PNIPAM-co-polystyrene core-shell microgels: Structure, swelling behavior, and crystallization. *Langmuir* **20**, 4330–4335.
39. Ceska, G. W. (1974). The effect of carboxylic monomers on surfactant-free emulsion copolymerization. *J. Appl. Polym. Sci.* **18**, 427–437.
40. Mcgrath, J., D. Bock, M. Cathcart, and A. Lyon. (2007). Self-assembly of "paint-on" colloidal crystals using poly(styrene-co-N-isopropylacrylamide) spheres. *Chem. Mater.* **19**, 1584–1591.
41. Pelton, R. H. (1988). Polystyrene and polystyrene-butadiene latexes stabilized by poly(N-isopropylacrylamide). *J. Polym. Sci. A Polym. Chem.* **26**, 9–18.
42. Duracher, D., F. Sauzedde, A. Elaissari, A. Perrin, and C. Pichot. (1998). Cationic amino-containing N-isopropyl-acrylamide–styrene copolymer latex particles: 1-Particle size and morphology vs. polymerization process. *Colloid Polym. Sci.* **276**, 219–231.
43. Brinker, C. J., and G. W. Scherer. (1990). *Sol-Gel Science: The Physics and Chemistry of Sol-Gel Processing*. San Diego: Academic Press.